Hindawi
Advances in Civil Engineering
Volume 2020, Article ID 8828819, 15 pages
https://doi.org/10.1155/2020/8828819

Research Article

Failure Mechanism and Kinematics of the Deadly September 28th 2016 Sucun Landslide, Suichang, Zhejiang, China

Hai Tian, Jianjun Gan, Hui Jiang, Chun Tang, Changtai Luo, Chenghui Wan, Bin Xu, Faliang Gui, Chengyi Liu, and Nian Liu

National-Local Joint Engineering Laboratory of Water Engineering Safety and Efficient Utilization of Resources in Poyang Lake Watershed, Nanchang Institute of Technology, Nanchang 330099, Jiangxi, China

Correspondence should be addressed to Jianjun Gan; 2014994522@nit.edu.cn

Received 1 August 2020; Revised 11 September 2020; Accepted 22 October 2020; Published 27 November 2020

Academic Editor: Chong Xu

The formation and dynamic process analysis of the rockslide avalanche in mountainous areas are one of the consequences of the catastrophic accident. Such loose accumulation in upslope may saturate partially or completely when the stability of their accumulation dam is distributed or affected by rainfall. We present a case study with respect to the southern Wuyi Mountain located in eastern China, where the wet and rainy climate has led to dozens of similar rockslide hazards. The purpose of this paper was to analyse the mechanism and dynamic characteristics of the rockslide influenced by the same geological conditions and to predict the outburst susceptibility of similar landslides in the future. Detail field surveys, 3D laser scanning, and high-density electrical methods were used to collect the geotechnical information of the complex landslide, to identify the discontinuity between the landslide material and the bedrock, and to investigate the deformation characterization and dynamic process of the rockslide. Based on remote sensing interpretation and field investigation of the deformation process of a landslide in different times and different parts, the background, mechanism, and cause of the landslide were demonstrated. The landslide is controlled by the characteristics of the geological structure, including collapse, circular sliding, plane sliding, and debris flow. In addition, there are rock avalanches on the rear edge of the slope subjected to the combined action of rainfall and gravity. Moreover, there are some resistance anomaly areas of the aquifer and soil between 2 and 50 m where the resistivity is less than 120 ohm-m, and they were deduced to be full of water, confirming a "bathtub" type structure. The mechanism of the catastrophic landslide was a combination of the upper pushing deformation induced by rainfall line uplift and rotational; due to the ancient landslide reactivation in the transposition area, the velocity of the rockslide reached 40.11 m/s.

1. Introduction

Studies of the geotechnical characteristics and dynamic process of rock avalanches can lead to a better understanding of landslide deformation and failure, and there are many case studies on rockslide avalanches [1–6]. Some important features of high rockslides, e.g., sliding depth, sliding distance, and deposit thickness, are not only helpful in quantifying the dynamics and stability evaluation of landslides but are also beneficial for mitigating landslide exploration, design, construction, monitoring, and early warnings [7]. However, it is usually difficult to determine whether internal deformation or boundary slip dominates under the combined influence of rainfall, earthquake, and complex geological conditions [8, 9]. Hence, some researchers have tried to analyse the background, characterization, and causes by multiple methods that used field surveys that include outcrop studies, geophysical exploration, drilling, geophysical exploration, and 3D laser scanning to analyse the characteristics and key factors causing rock avalanches [10, 11].

Rock avalanches are usually caused by the initial outburst from the numerous rock mass with fast movement during transportation [12, 13]. It reflects that the complex features of rock avalanches are due to the complexity of the formation mechanism and large-scale size for rock mass.

Such rock avalanches often lead to catastrophic events because of their large speed. Based on numerous case studies, many further and deeper works on rock avalanches, especially the formation characteristics and genetic mechanism of rock avalanches, have been performed. Moreover, some new technologies and methods, such as numerical simulations, 3D scanning, satellite remote sensing, unmanned aerial vehicle (UAV), and interferometric synthetic aperture radar (InSAR), have been applied to study large-scale rock avalanches [13–20]. However, multiple methods include traditional investigation methods and new monitoring technology to analyse the mechanism and cause of a landslide, which are important for the in-depth study of this type of landslide [21].

At 15:28 on September 28, 2016, a large-scale catastrophic landslide occurred in Suchun village, Beijie township, Suichang county, Zhejiang, China (N 28° 47' 03", E 119° 18' 13") (Figure 1). This landslide washed away and buried the village below, forming a barrier lake with an area of approximately 35.2 km^2, killing 27 people, destroying 31 houses and 450 m of the highway, and blocking the creek at the slope foot. The landslide could be divided into two zones: a sliding collapse zone (located in the upper upslope, approximately 220 m long, 190 m high, and 70–150 m wide) and a sliding accumulation zone (located in the frontal of the slope, approximately 750 m long, 300 m high, and 100–340 m wide).

Due to the frequent occurrence of rapid rock landslides in the Zhejiang province and serious damage and economic losses they cause, some scholars used field investigation [22], GIS method [15, 23], SAR technology [16], physical simulation technology [24], and the probabilistic method [25] to analyze the rock slope stability and discussed the dynamic characteristics of the landslide debris flow. However, these studies seldom consider the effect of many factors on the landslide, such as the internal geological structure, particle composition, and variation of the groundwater level.

To more truly understand the internal causes of rock landslides and truly reflect the relationship between landslides and the geological structure, stratigraphic lithology, water level changes, and other factors, we have used field investigations, high-density electrical methods, and numerical analysis. Various methods were used to study the landslide. Through these multiple methods, we found the sliding mass was relatively thin in the middle part of the slope, and 5–10 m of rock soil aggregate covered the granite bedrock. According to historical records, in 1340 AD, a massive landslide occurred in Sucun, damaging 53 residential houses and killing more than 360 people. Since May 19, 2010, when a 3000 m^3 landslide occurred in the area and monitoring began, the landslide has been slowly deforming year by year. A similar catastrophic rock avalanche near the Suichang county occurred in Lidong village at 22:50 on 13 November 2015 and caused 38 fatalities (Ma et al., 2015), which is a recent example of this widespread problem.

2. Geological Background

The Sucun rock avalanche occurred in the northeastern area of the Wuyishan-Xianxialing range, Sucun, Suichang county, Zhejiang, China, and Sucun is located at the foot of the slope. The village was well known for leisure agriculture and rural tourism which was located at the junction of Zhejiang, Jiangxi, and Anhui provinces (Figure 1).

The ridge at the research landslide area is 340–871 m high, and the upper terrain's angle gradually decreased to 30°~40° under the steep crown of the scar; the lower terrain is 15°~25°, and the slope aspect is 225°. The position of the study area is located on the northeast side of the landslide, with an elevation of approximately 965.5 m. The lowest point is located at the bed of Taoyuan creek, where its elevation decreased to 296.4 m. The exposed strata in the landslide area are mainly loose quaternary deposits and Yanshanian intrusive rock. The loose accumulation layer is composed of eluvial deposits ($Q^{el\text{-}dl}$), colluvium (Q^{col}), and landslide deposits (Figure 2).

Rocks of medium-coarse-grained monzogranitic porphyry and porphyritic fine-grained granite outcrop are found in the landslide area. Medium-coarse-grained monzogranitic porphyry ($\eta\gamma_5^2$): light fleshy red, porphyry structure, and massive structure outcropping on the southwest side of the landslide. It is also widely distributed in the upper and middle slopes. Porphyritic fine-grained granite (γ_5^3): outcropping along the northwestern part of the landslide, composed dominantly of flesh red and porphyritic fine-grained granitic structures, and the structure is massive. Two faults that differ from several rock joints are well developed in this rock group, and the rock was broken off the slope surface (Figure 3).

This rockslide accelerated along two bedding bedrocks in a different direction. A rock avalanche with a volume of 24×10^4 m^3 accelerated along the 36° southwest-dipping bedding zone (I). This rockslide swerved when it was deflected by a hard rock wall on the west side, causing the older avalanche deposits on the breakaway zone accelerated along 18° southeast-dipping bedding bedrock (II). A secondary anticline with largely broken shales was found to the southwest in the middle of the landslide area. These are only part of the geological background for the two accelerations because several staggered faults remain in their position.

The spatial distribution and assemblage of these faults are very complex results in the unique geological environment of the landslide area. As shown in Figure 3, the main faults in the area are the Quzhou-Suichang NW trend deep fault zone, and the Sucun landslide is located approximately 15 km from the deep fault zone. The unstable slope is characterized by 3 tectonic faults and 114 joints. The fault characteristics in the landslide areas vary greatly. The F1 fault located on the west side of the scarp turns from W 15°–20° S/EN 50°–60°. Likewise, the attitude of the F2 fault on the same position is W 21°–25° N/WS 82°–87°. However, the F3 fault dips at 61° into the consequent rock slope towards N 30°W and is approximately 180 m from the scarp, forming a cliff with a 61° angle. This suggests that the formation of the rockslide seems to be closely related to the cataclastic process in the three fault zones, which provides a unique source of thickened rockfall deposits for the landslide.

Climate change may affect the intensity and frequency in this rainfall-induced landslide area, thus increasing the

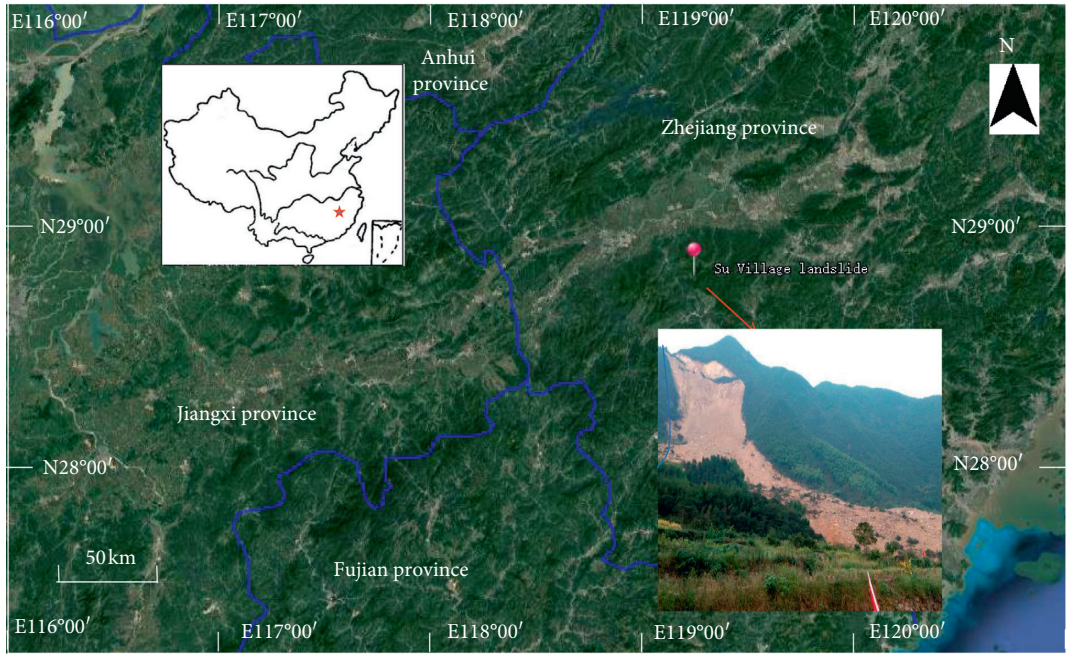

Figure 1: Location of the Sucun landslide in the Suichang county.

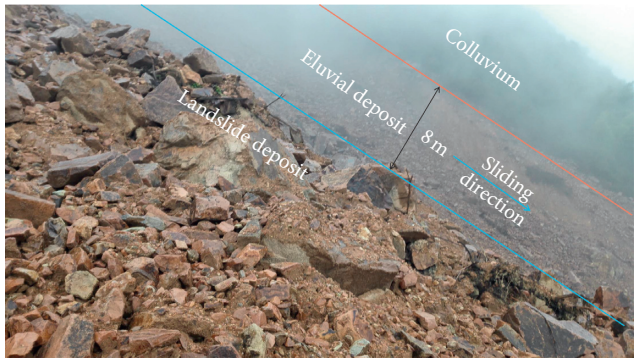

Figure 2: Postlandslide accumulation in the middle part of the slope (this photo was taken at 9:15 am, 30 September 2016, two days after this rockslide occurred, when the upper part of the landslide was covered by cloud).

probability of the catastrophic events. Since the study area has a subtropical climate, the average temperature over the past 40 years is 17.60°C, and the annual rainfall is approximately 1515–1878 mm. Taoyuan creek at the slope foot of the landslide area has a perennially flowing ditch. According to the monitoring data from the neighbouring Wangzhaiqiao raingauge station (approximately 1 km from Sucun) from September 28 to October 5, 2016, the total rainfall during the process was 189.8 mm, and the maximum daily rainfall was 127.2 mm (on September 28, 2016). Pore water pressure may change with rainfall and thus controls the strength of the upslope rockslide deposit in the head (collapse area).

The development of the Sucun rock avalanche may be closely related to its topography. Since the landslide has a bedding slope with a strata dip angle from 45° to 85°, where the tendency is SN, whereas a locking segment (tendency NS) is formed with a dip angle from 11° to 16.8° in the head of the landslide. Therefore, at the toe of the main scarp, a concave topography is formed. In terms of geological structural control, there are two cross-cutting steep joints that may be the key to the generation and development of the landslide source. Joint set 1 tends toward WS (W10°S~W50°S) and dips at 50~80°; close to the vertical, its overall attitude is nearly parallel to the F1 fault attitude, forming a main fracture rock-mass structural plane in the landslide area. As a result, joint set 1 forms the northern slope face, nearly parallel to the northern cliff. The other dominant joint set 2 has the orientation of the NW (N20°W~N50°W) and dips in the 75°–81° direction. The joint set is like a plough, with a density of 1~3 strips/m, generally without filling, with an extended length of 1~3 m, and locally reaching more than 10 m. Figure 4shows the two dominant joint sets intersect each other thus creating some near-vertical scars and rock faces at both sides of the sliding area. The cross-cutting of these two joint groups breaks the older rockslide deposit structure in the head, accelerates the formation and accumulation of landslide debris at the rear edge, and provides a large number of material sources for the start of the landslide. Therefore, once the deposit in the source area exceeds a certain thickness, it is easy to trigger a landslide under the influence of rainfall infiltration or human engineering activities [26, 27].

3. Data and Methods

In this paper, according to a surface observation and geological survey investigation, the geological conditions, geomorphological features, and deformation processes of the Su Village rock avalanches have been introduced firstly. Then, by applying 3D laser scanning, high-density electrical resistivity topography (HDERT), and 3D numerical

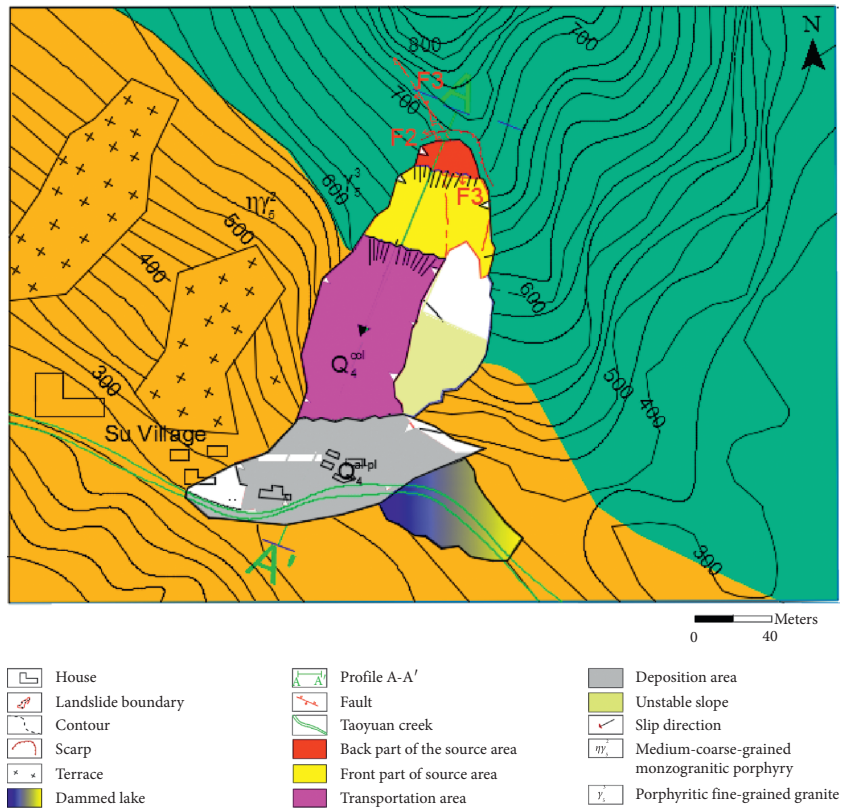

Figure 3: Schematic geological map and landslide feature of the Sucun rock avalanche.

modelling, the genetic mechanisms, characteristics, stability, and dynamics of the landslide were analyzed.

Figure 5 shows the developed multitechnique investigation of very fast-moving rockslide avalanche as well as the relation between different work steps of the research carried out. The technique presented includes four main stages.

The first stage includes field investigation which includes casing drilling and high-density electrical resistivity topography (HDERT). While the field investigation dealt with the study of the geological background such as topography, geological structure, stratigraphic lithology, and hydrogeological condition in the study area, the HDERT was used to determine the geotechnical structure, groundwater level, sliding zone, and the cause of the rockslide.

In the second step of the study, historical aerial photograph analysis and three-dimensional deformation analysis are carried out. From the historical aerial photograph of the study region, the process of landslide development and evolution can be understood, and also, the runout parameters can be provided for studying the formation mechanism of the landslide. The comparative analysis are conducted by the comprehensive information with respect to the different years (2010, 2013, 2016, and 2017), including the topography data from the satellite remote sensing and aerial photos in a large scale (1:500). In order to quantitatively analyse the deformation and failure characteristics of the landslide after deformation, the collapse area, movement area, and accumulation area are divided scientifically. The 3D scanning equipment with accuracy up to cm level was used to monitor and receive the terrain data of the landslide area. Thus, integration and conjunction of the topography data with the data from the satellite sensing and 3D scanning method have been achieved.

In the third step of the study, the runout characteristics of the study area were analyzed by field investigation and theoretical calculation. Field investigation is to verify the satellite remote sensing data and the data obtained by 3D scanning. Based on the results of image interpretation and field investigation, the landslide is divided into four subareas: source area, transposition area, deposition area, and potential source area, and then the deformation and failure characteristics of each area are analyzed. Data have been provided from the field investigation, satellite remote sensing, and 3D scan, so the theoretical method is mainly based on the empirical formula and the topographic data obtained from the investigation to calculate and predict the kinetic characteristics of the landslide.

4. Results

4.1. Characteristics of the Landslide. According to QuickBird's remote sensing image in 2010 and 2013, the landslide is located in northeastern Sucun, Beijie township, and the top of the landslide is in Huashangjian. The back edge is a depression of landslide accumulation. The field survey and remote sensing images show that the middle slope is a steep valley bedding slope, and the front edge is Taoyuan creek and riparian farmland. A semicircular arc tension crack is

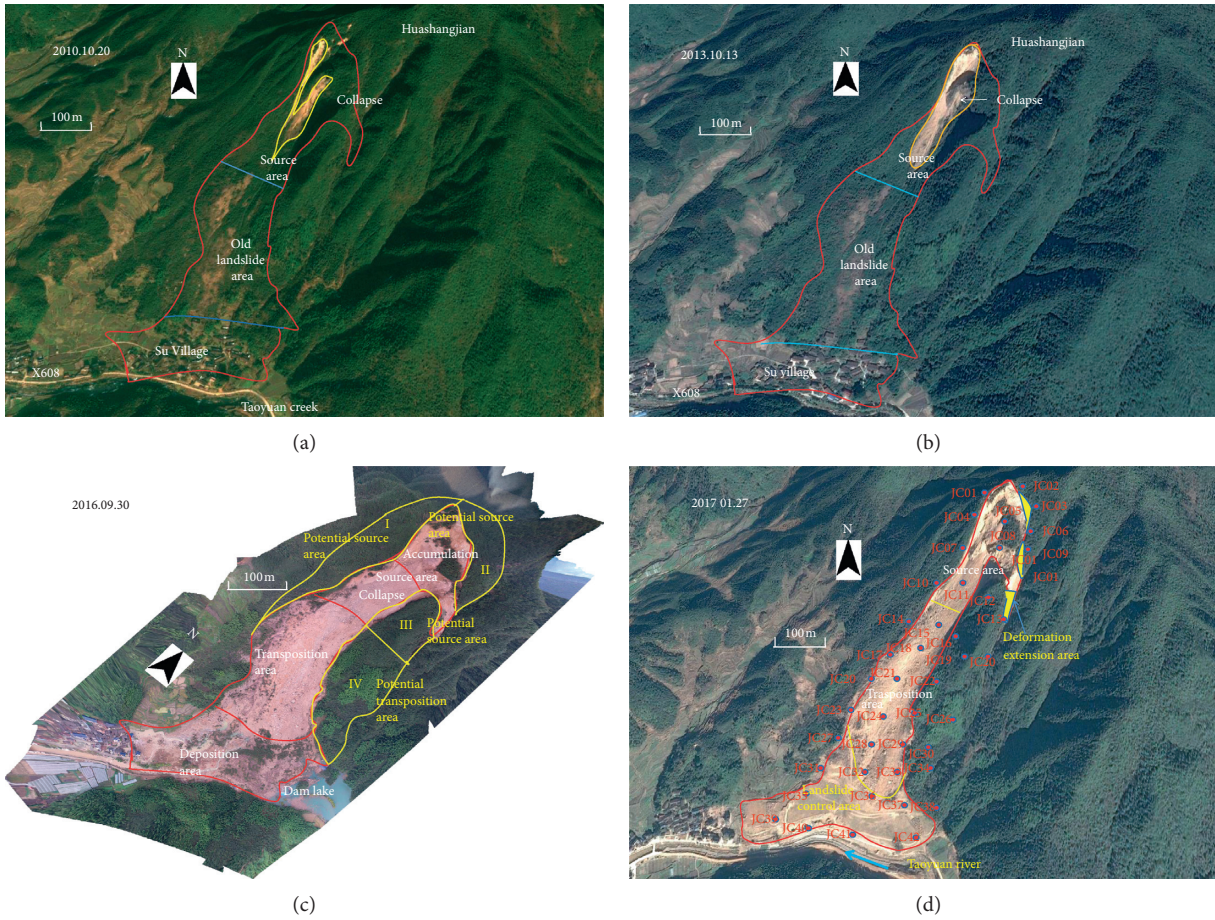

Figure 4: Photographs of the Sucun landslide. (a) Image was taken on October 20, 2010 (from Google Earth). (b) Image was taken on October 13, 2013 (from Google Earth). (c) Aerial photograph was taken on September 30, 2016, and subdivided landslide. (d) Image was taken on January 27, 2017, and distribution of monitoring points (from Google Earth).

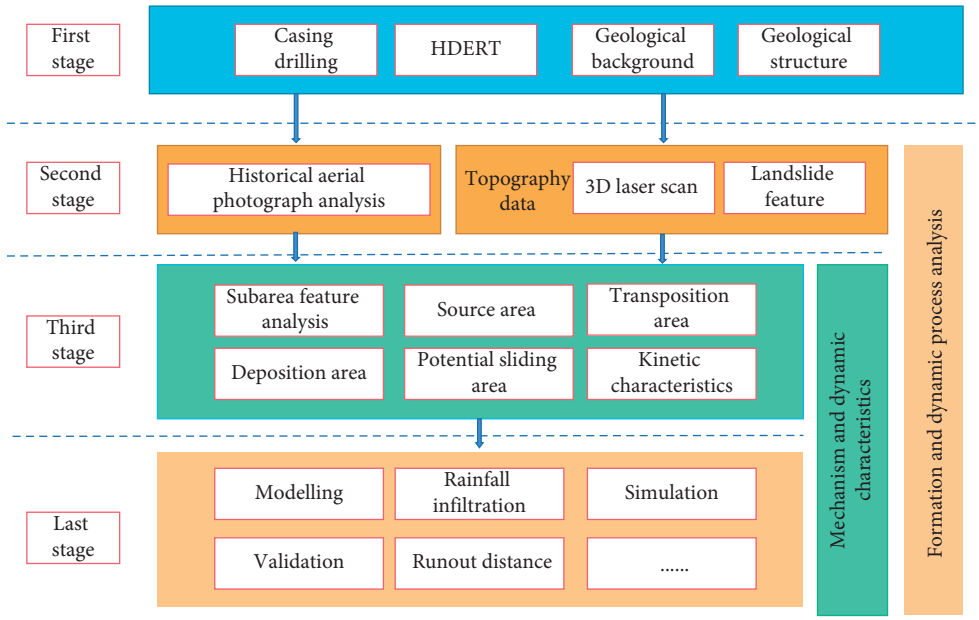

Figure 5: Methodology for the formation and dynamic process analysis.

distributed on the back edge of the landslide, which is intermittent, with some downfaulting and connectivity. The front edge is a protruding steep rock wall. The left margin of the failure slope coincides with a catchment gully, and the right edge of the landslide is a ridge. The X608 county road passes through the foot of the landslide (Figures 4(a) and 4(b)).

In October 2010, a small-scale rockfall or collapse occurred in the southwest part of Huashangjian, which formed a scarp north of the collapsed accumulation area (Figure 4(a)). After October 2013, the collapse area distinctly increased with progressive increase of rockfall volume along the downslope direction. Based on this surface failure phenomenon, some local geology experts concluded the slope may be a potential geological hazard. On September 26, 2016, due to the typhoon warning, a temporary shelter for the Sucun residents was set up by the local government, and it was recommended that they stay in the temporary shelter at night. Unfortunately, at that time, nobody predicted that such a high-speed and large rock landslide would occur so quickly, and it burst during the day (Figures 4(c) and 4(d)).

After the landslide disaster, 42 surface displacement monitoring points were set up in the landslide area. The monitoring results show that the slope was still in continuous deformation until January 27, 2017, but the deformation rate tended toward stability (Figure 4(d)). According to various geological conditions and topographic characteristics, the Sucun landslide is divided into the source area, transposition area, deposition area, and potential source zone. The potential source zone is further divided into potential source area (I), potential source area (II), potential source area (III), and potential transposition area (IV) (Figure 4(c)). The characteristics of each area of the Sucun landslide are shown in Table 1.

4.1.1. Characteristics of the Source Area. Within one month before sliding, movement in the back of the source area became more continuous. A field investigation and satellite remote sensing images on July 8, 2016, show that the crack at the back edge of the landslide continued to expand, connect, and dislocate, and the peripheral boundary of the southwest side of the landslide body was preliminarily formed (Figure 6(a)). On September 26, 2016, the southwest boundary was connected with the rear edge (Figure 6(b)), and the collapsed area was extended well to the foot of the steep slope front, and the eastern gulley in the back slope was connected.

At approximately 3:28 pm on September 28, 2016, after the long-term accumulation of the fall in the rear part of the slip area, a rock mass of approximately 240,000 m^3 deposits was added at the back part of the slope. Moreover, according to the failure characteristics of the rockslide avalanches, the collapse zone has been subdivided into two subzones: the collapse zone and the accumulation zone. The steep slope of the landslide is the trailing edge collapse area, the elevation difference is 30~60 m, and the slope is 50° to 60°. There is an old collapse (YH1) west of the source area, with a volume of approximately 135,000 m^3, which is an important material source of the Sucun landslide. Under the action of rainfall infiltration, rock avalanches originated in the collapse deposits disintegrated rapidly and dipped along over 30 m of high steep slopes into the middle and front of the slope.

After the landslide, the scale of the source area was extended to 220 m long and 70~150 m wide, and its total area was approximately 205,000 m^2. Because the failures of the YH1 and YH2 rock collapses entrained and liquefied the saturated soil in their paths, a large amount of the loose deposits was displaced from the margins of the source area. Besides, the substrate material that smeared along the base of the deposits, liquefied soil extrusion upward through the deposits, and volume increases in the cave topography may all be essential factors in the rotational slides in the source area [8]. By referring to field investigation and preslide photos to recover the preslide terrain, the total volume of moving material in the source area was estimated to be approximately 340,000 m^3 (Figure 7).

4.1.2. Characteristics of the Transposition Area. Through multimethods including field investigation, high-density resistivity topography, 3D laser scanning, remote sensing, and borehole drilling, we found that the macroscopic deformation in the transposition area mainly shows two phenomena: cutting on both sides and scouring in the gully. The western boundary mainly consists of oriented rocky landslide deposits (Q_4^{del}) and fine-grained granite (γ^3). The fresh-cut slope is approximately 8 m high, which implies that any scratch rock is hit by high-speed rock avalanches (Figure 8(a)). However, the eastern boundary of the landslide is mainly composed of the slope deposit and medium-coarse-grained monzogranitic porphyry ($\eta\gamma_5^3$), and the fracture is nearly parallel to the sliding direction at depth along the pre-existing joints (Figure 8(b)). Like the Vajont slide, the topography of the transposition area is similar to a chair shape in the middle part of the slope. Similarly, steep rock failure in the minor scar at this transposition area often involves an acceleration lateral release with the rotational movement of the Sucun landslide, resulting in a complex kinematic release. . By the 3D laser scanner method, detailed DEM data of the key position have been provided to study the dynamic characteristic of Sucun. The current elevation of this area ranges from 320 to 620 m. The longitudinal length is approximately 550 m, and the transverse width is 100~340 m, so the area is approximately 99,000 m^2. Rock avalanche deposits, in which the volume in the transposition area is approximately 270,000 m^3, have the stacking thickness up to 12.0 m (Figure 8(c)).

Comparing Figures 4 and 6 shows that large rock avalanches had been spread from the main scrap during this short interval. The massif of these avalanches is mainly composed of fleshy red fine-grained granite in the γ^3 layer and the red-gray-red medium-weathered coarse-grained monzonite in the $\eta\gamma_5^2$ layer. The back scarp in the transposition area mainly traced joint set 1, trending nearly

Table 1: The characteristics of different areas of the Sucun rockslide avalanche.

Landslide area	Subarea	Location	Length (m)	Width (m)	Volume (m^3)	Gradient (°)	Area (m^2)
Source area	Accumulation area	Head	120	70–150	135,000	60–70	10,000
	Collapse area	Front part of the landslide	100	100	205,000	50–60	11,000
Transposition area		Center of the landslide	550	100–260	270,000	10–25	99,000
Deposition area		Toe of the landslide	200	230–430	930,000	0–10	66,000
Potential area	I	Upper western side of the source area	320	70–90	96,000	25–30	24,000
	II	Upper eastern side of the source area	150	60–80	105,000	28–35	10,500
	III	Upper eastern side of the transposition area	100	80–100	72,500	15–25	9,000
	IV	Lower part of the eastern side of the transposition area	280	50–120	179,200	10–25	22,400

(a) (b)

Figure 6: Avalanche movement continuous in the back of the source area. (a) Photo was taken on July 8, 2016. (b) Photo was taken on September 26, 2016.

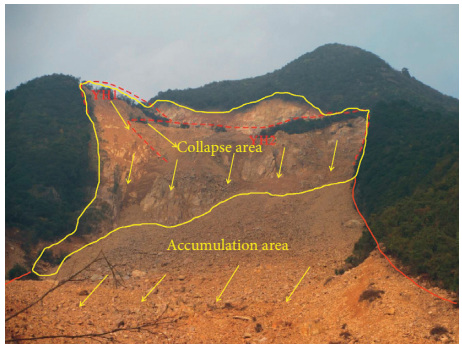

Figure 7: The source area is a "chair-like" topography after sliding at the Sucun landslide (it was taken on September 29, 2016, by the third geological team of the Zhejiang province).

W70°N and dipping 50°towards NW. Figure 8 shows that the exposed crushed rocks in this area were larger than those in the source area, which means that these new landslide boulders are formed by large potential energy and cover from the ancient landslide.

On the western boundary in the transposition area, small-scale collapses in the range of 100~1000 m^3 occasionally occur. Sometimes, there are several breakdowns in a day. Through the analysis of satellite images and 3D laser scan monitoring data, the main steep slope continues to collapse. Our investigation revealed the fundamental role played by the rupture surface is featured by shear strength deterioration of the weak interlayer rather than a fracture of the shallow rock avalanche. Controlled by the original stratigraphic structure, the weak interlayer is composed of the clastic clay containing the crushed stone. This weak interlayer is located between the strongly weathered layer accumulation and the top surface of fully weathered granite and has high deformation capacity and high energy dissipation. This is a weak layer whose strength tends to decrease rapidly, and it is approximately 50 cm thick and composed of clastic minerals and potassium feldspar. Because of the loose structure, when we drill to sample, it is difficult to remove a complete sample.

4.1.3. Characteristics of the Deposition Area. Figures 4(c) and 6(a) show that the morphology and volume at the deposition area are most likely explanation dynamic characteristics of high-energy fragmentation spreading rockslide. Its longitudinal length from the foot to the toe was 230 m, and widths of the rockslide deposit vary from 120 to 430 m. Rockslide deposits covered 66,000 m^2, with an average thickness of 14.7 m, and its volume we calculated is 970,000 m^3. All these loose materials which are spread over

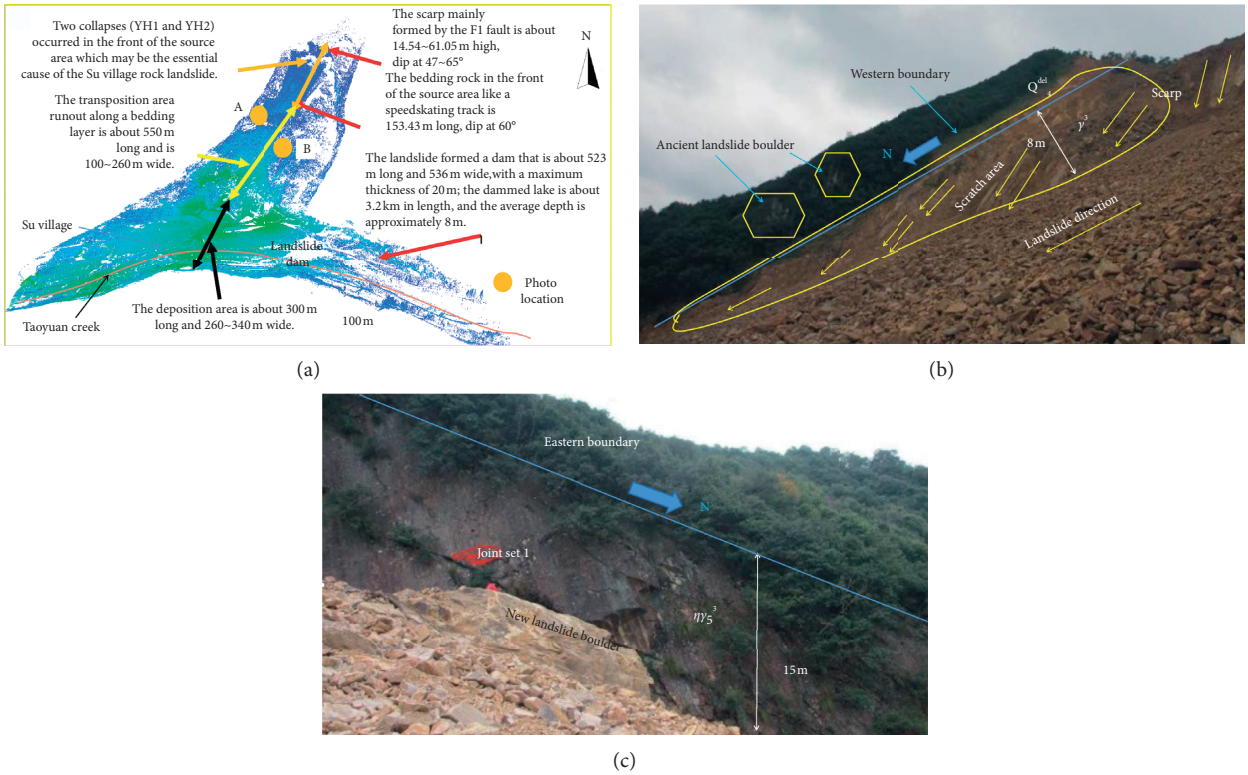

Figure 8: Photograph by a 3D laser scanner and the transposition boundary. (a) 3D laser scanner topography. (b) Western boundary of the landslide with some scratches and fresh-cut steep slope. (c) Eastern boundary of the landslide with well-developed joints and a fracture that is nearly parallel to the slide.

the deposition area have uniform particle sizes, resulting in both unique sedimentary characteristics and dynamic characteristics. Note that a unique binary structure, consisting of coarse particles near the upper surface and fine particles on the bottom, was proposed bySosio et al. [28], who used the Voellmy model to simulate the increase in rock avalanche deposition volume and predicted the characteristics of the deposition area [29].

According to drilling and high-density resistivity topography, the material in the deposition area is a fine-grained granite block deposited mainly in the toe. However, coarse-grained monzonitic granite, rhyolite, and basaltic porphyrite can also be seen sporadically in the deposition area; generally, the particle size is 0.5~1.0 m, and the maximum particle size is 10 m, which indicates that the upper rocks are diverse, loose in structure, and active in the geological structure (Figure 9). Besides, a sand layer with a maximum thickness of 5 m developed under the rock deposit, and we deduced that the sand layer was always in the toe of the slope, which originated from the ancient landslide deposit. The foremost granite moving directly over Taoyuan creek created a cross-valley dam and climbed onto the opposing bank. Here, the rock avalanches formed a barrier lake and blocked the upper creek over 20 m. Houses, farmland, and highway in this area were destroyed by the impact and collision with these rock avalanches, which suggested that the sliding materials traveled with a very high velocity.

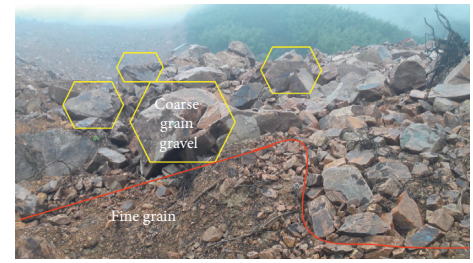

Figure 9: The deposition area is composed of large blocks having a binary structure. View of the rockslide deposits showing the upper slope composed of coarse grain gravel and fine-grain debris flow deposit located below.

Through field surveys such as drilling and 3D scanning techniques, we estimate the total volume of the Sucun landslide is about 154,000 m^3, include deposit in the source area (34,000 m^3), transposition area (27,000 m^3), and deposition area (97,000 m^3). Approximately 154 million m^3 of granite blocks slide along the weak clastic clay and crushed stone interlayer according to the above survey analysis. The sliding body changes from slow motion to a fast downward motion from the top of the slope, and the sliding accelerated along the 800 m long bedding rock and across Taoyuan creek at the slope toe. Blocked by the opposite creek bank and forming a barrier dam of 523 m long and 536 m wide in the avalanche mode, a new accumulation body with an average thickness of 8 m was ultimately formed.

4.1.4. Potential Source Zone. Figure 4(c) shows that the outline of the potential slide area is like an oval. The potential slide area is in the upper part of the landslide, and the area is divided into three subareas based on the failure characteristics. The main deformation is concentrated on the eastern boundary of the slope and the back edge of the source area. Many vertical and horizontal cracks were created due to the steep terrains in these unstable slopes, and below these cracks, failure may occur along with one of the suitable discontinuities based on various geological conditions and topographic features; the potential area is split into the following subareas:

(1) The scratching area along the western boundary head is defined as area I in Figure 4(c)

(2) The collapse area at the back (north) head is defined as area II in Figure 4(c)

(3) The potential source zone along the eastern boundary of the landslide, which is defined as areas III (potential source area) and IV (potential transposition area) in Figure 4(c)

Characteristics of scratch area I: from the field investigation and by interpreting the remote sensing images along the western boundary of the source area before and after sliding, which are shown in Figures 3 and 7(a), we assume that the rock avalanche began quickly and accelerated across the steep slope in front of the source area and then traveled downslope with a high velocity. However, the contribution of a massive deposits or ancient debris in the transposition area will lead to large-scale landslides. Evidence of these high-speed movements can be seen in the sharp scratches on some slopes (Figure 7(a)). Potential area I looks like a shuttle with an area of approximately 16,000 m^2. From 1st November to 12th December 2016, horizontal displacement monitoring points JC07 and JC10 showed average daily increases of 0.77 mm and 0.28 mm, respectively. The total vertical displacements that occurred at points JC07 and JC10 during the same time are 59 mm and 18 mm, respectively. Among these, from 16th November to 19th October 2016, the horizontal displacement at monitoring points JC07 and JC10 increased by 4 mm per day and 3 mm per day, respectively. From 1st to 5th November 2016, the total horizontal displacement at point JC07 increased by 14 mm. From 5th to 12th November 2016, the total cumulative settlement at monitor point JC10 increased by 12 mm (Figure 10(a)).

Potential collapse area II: the collapse area (area II in Figure 4(c)) is the left lung-shaped area located at the back of the landslide source area. Some cracks were formed in this area due to the faults (F1, F2, and F3) and joints (joint set 1 and joint set 2) and covered a total area of approximately 15,000 m^2. As a result, the rock blocks cut by crisscrossing joints are prone to collapse along with the cracks under the action of gravity and accumulate in the concave ground of the source area. From November 1 to December 12, 2016, the total horizontal displacements at monitoring points JC02 and JC05 were 39 mm and 65 mm, respectively, and the average daily displacement at points JC02 and JC05 reached 0.73 mm and 1.12 mm, respectively. The total settlement displacements at monitoring points JC02 and JC05 were 20 mm and 22 mm, respectively, from November 1 to December 12, 2016 (Figure 10(b)).

Potential source area III: according to the satellite image and field investigation, we can see that the failure materials gradually stopped and deposited in its position with the energy dissipation. Figure 4(c) shows that this area was between two gullies: the western gully of this area is a cliff with an average height from 2 m to 15 m; the eastern gully is an active gully with a collapse and a rock slide that were extended to a slope of approximately 15 mm from September 26 to December 12, 2016 (Figure 4(d)). Rocks in this area are predominantly large bedding "pure" rock fragments, which cover an area of approximately 15,500 m^2. The thickness of the potential slide rocks varies in the space because of their complex geological conditions. Affected by the strong weather, rainfall infiltration, and erosion and deposition by gravity, the rocks in this area slide down in the same direction. According to the data of monitoring point JC13, from 1st November to 12th December 2016, the horizontal displacements were between 17 mm and 79 mm, with a high rate of 1.52 mm per day. The total ground surface settlement at point JC13 ranged from 9 mm to 60 mm, with a rate of approximately 1.21 mm per day (Figure 10(c)). Both the accumulated displacement and settlement increased in the back part of the potential source area (III), suggesting that the loose deposit on the surface of the unstable slope is still in creep deformation under the influence of gravity and rainfall infiltration. It can also be seen from Figure 10 that the horizontal displacement is approximately positively correlated with rainfall, while the subsidence displacement is approximately negatively correlated with rainfall accumulation. During the monitoring period, cumulative rainfall in the study area continued to increase, leading to an increase in both horizontal and subsidence displacements.

Potential transposition area (IV): this area is located in the lower half of the east-facing unstable slope area (Figures 4(c) and 10(d)). We infer that the granite deposits were always deforming in this area during the sliding process, which may be downslope along with the bedding rocks. From 1st November to 12th December 2016, the horizontal displacements at monitoring point JC22 were between 5 mm and 21 mm, with a very small rate of 0.18 mm per day. Simultaneously, the horizontal displacement at point JC30 was between 2 mm and 15 mm, with a low rate of 0.30 mm per day. The total settlement displacement at both points JC22 and JC30 was between 1 mm and 8 mm, with a very small rate of 0.18 mm per day. The displacement change curve in Figure 10(d) shows that the monitoring data have no changes between the monitoring periods, which indicates that the point may be a stable slope.

4.2. Kinetic Characteristics of the Sucun Rock Avalanches. Most rock avalanches in high mountain regions result from the rapid fragmentation of very fast movement, caused by the rapid breaking up of an initially intact rock mass [8]. Such fragmentation is known as a rock avalanche with a large volume (often more than 1 million m^3) of bedrock

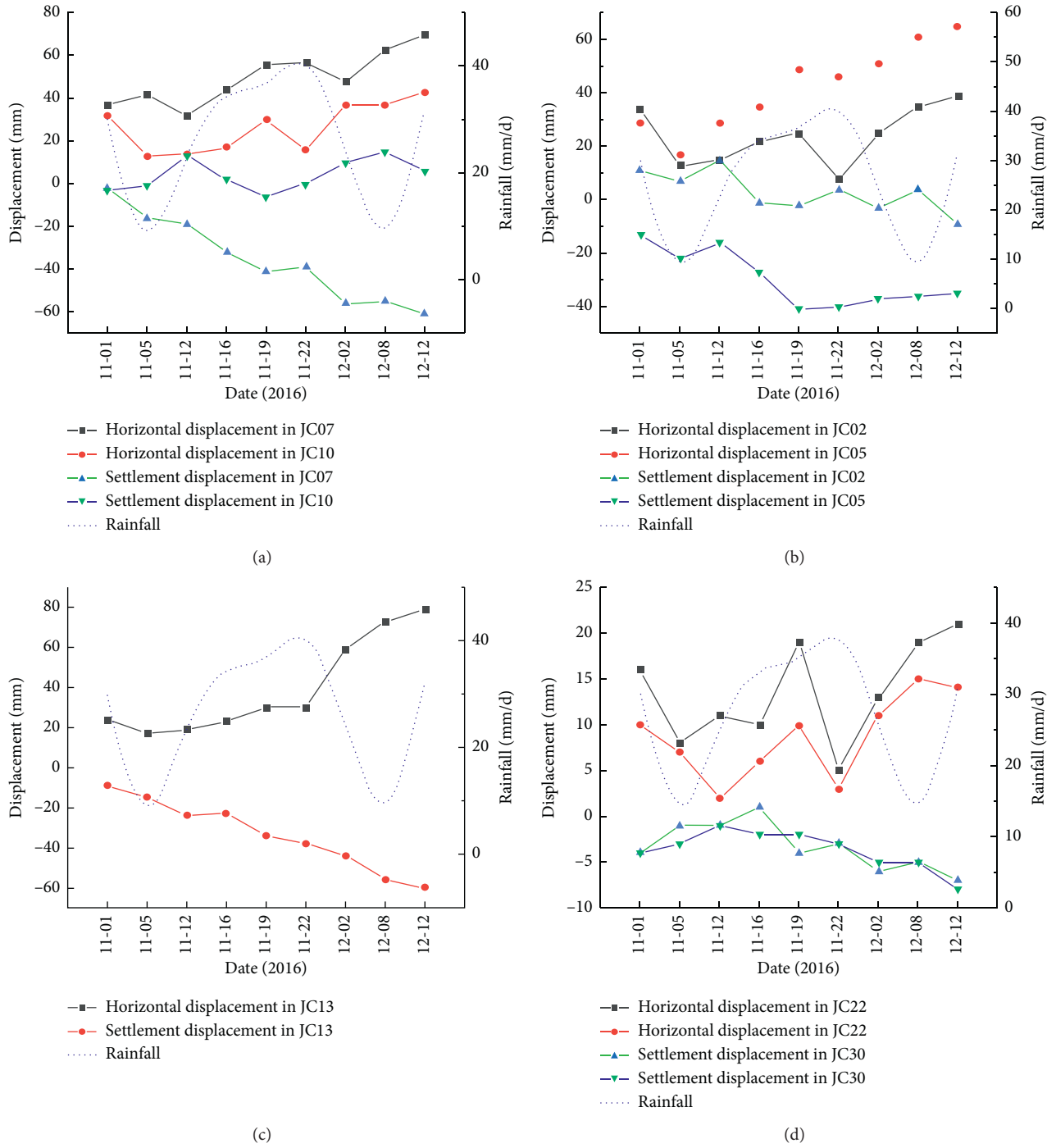

Figure 10: Monitoring data of the potential slide area for the Sucun landslide.

mass movement, which creates overburden stress that is termed "sagging" which causes dynamic fracturing of the subsurface in the slope. Some avalanches have occurred repeatedly in the same rock location after hundreds of years due to catastrophic geomorphic processes [30]. It is necessary to analyse the dynamic characteristics of such landslides for geological disaster prevention; their formation mechanism analysis allows the kinetic characteristics of rock avalanche failure movement to be reconstructed. The travel distance, velocity, and depositional thickness are important parameters used to describe landslide movement characteristics. Generally, the methods for predicting a rock avalanche motion can be divided into main facies: (1) the empirical-statistical model, which should only be applied to conditions similar to those of development, and these models are more useful for predicting L (the runout distance of the rock avalanche) than s (the velocity of the rock avalanche) (Dickenmann, 2005); (2) the numerical simulation

methods, including continuum and discrete methods, which are based on computer software (e.g., DAN3D, RAMMS, FLOW 3D, and PFC) [28].

In this paper, based on Adushkin et al.'s [31] data, Sucun rock avalanches are analyzed using the continuum-based method. Then, the important sliding parameters are analyzed by a numerical simulation. Adushkin et al. compared several landslides of different geneses and proposed a relationship between the rockfall stroke and its volume. Referring to this method, the main parameters and definitions of Sucun rock avalanches are shown in Figure 10. From this figure, we can see that the slope thickness centre of the gravity in the source zone (H^*) is approximately 435.49 m, and the maximum horizontal distance between the toe of the Sucun rockslide and the gravity centre of the deposit at the head (L^*) is approximately 1225.81 m. The average thickness of the landslide accumulation (h) is approximately 14.69 m, and the length of the rock avalanche accumulation (l) is approximately 606.44 m. L and H are approximately 1400 m and 486.11 m, respectively, based on the corresponding L/H value which is 2.88, and its volume is 1,540,000 m^3. Figure 11 shows that curve 1 denotes rock avalanche tests in Adushkin et al.'s study [31], curve 2 denotes natural rock avalanches, and curve 3 represents rock-ice avalanches. The blue dot in Figure 11 is close to curve 1 that denotes rockslide at Sucun is a good match with curve 1. Such dependence of rock avalanches L/H and V (volume) with $V = 10^6$ m^3 can be described by curve 1 (Figure 12).

The velocity of Sucun rock avalanches, based on energy transfer theory equation (1) [32], can be estimated by combining field investigation with theoretical. Because of the slight influence during the avalanche process, the effect of cohesion (C) could be ignored, so the formulas of movement velocity and acceleration of the rock avalanche could be written as follows:

$$v^2 = 2gh(1 - c\tan\phi\tan\alpha), \quad (1)$$

$$\alpha = g(\sin a - \cos a\tan\phi), \quad (2)$$

where v denotes the velocity (m/s); g denotes the gravitational acceleration; h denotes the height difference, which is approximately 385 m; α denotes the acceleration of the collapse or landslide debris flow; a denotes the slope angle, which is approximately 21.5° and is mentioned in Figure 11; and ϕ is the internal friction angle of the slip surface that is tested in the lab at approximately 42.5°.

Thus, the velocity was calculated as 40.11 m/s, which suggests that the Sucun rock avalanche that is very close to the value estimated by the video recording data (https://v.qq.com/x/page/g03334qjxj0.html), and the acceleration was 0.38 m/s^2. Based on an avalanche of landslide with flow type [8], this avalanche is an extremely rapid rock avalanche. Due to the high speed, an air-blast wave and cast dust cloud were produced during rock avalanche motion.

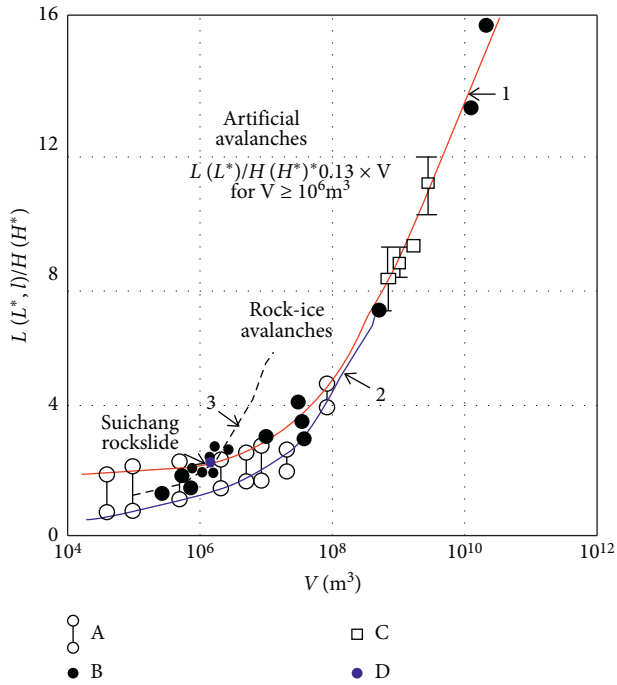

Figure 11: Relationship between the length to fall height ratio and volume of the rockslide (after Xu, modified, 2010): A, rockslide induced by earthquake or explosions. The upper curve represents the ratio of L^*/H^*, and the lower curve represents the ratio of l/H^*; B, rock-ice avalanches in the Khibini Mountains; C, volcanic rock avalanches; D, natural nonvolcanic rock avalanches.

4.3. The Cause of the Landslide

4.3.1. Formation Mechanism and Cause of the Sucun Rock Avalanche. Rock avalanches can be induced by gravity, rainfall, earthquakes, snow, and so on. Depending on the analysis of the topography and geometry of its substrate, the formation and causes of the Sucun rock avalanches can be summarized as follows: rainfall infiltration in the source area; weak and impermeable material in the subsurface; and vulnerable geological conditions. The main geological and geomorphologic evidence supporting this hypothesis is summarized as follows.

4.3.2. Rainfall Infiltration in the Source Area. Heavy rainfall during typhoon Megi (1617) caused the landslide in the Suncun village. The majority of slope instability is the result of rainfall. Rock avalanches are a response to rainfall that involves physical processes of strength loss at different time scales. Fundamentally, the continuous rainfall on record for the upper slope in Sucun, that of September 2016, is attributed to the dynamic failure of an older unstable landslide, resulting in an increase of the gravity for the collapse deposits, a decrease of the cohesion, and remoulding and liquefaction of the substrate. Once these parameters are changed, destabilization and failure of the slope may occur

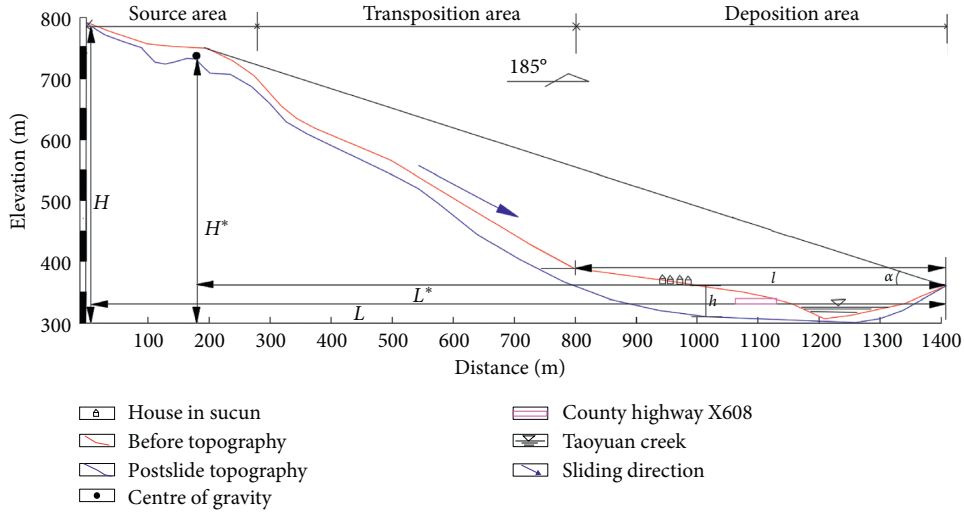

Figure 12: Parameters of the Sucun landslide (modified from Adushkin et al. [31]).

rapidly. According to the monitoring data from the local hydrological station, before the landslide occurred, 13 days of rainfall occurred in the study area in September 2016, with the maximum daily rainfall record broken on September 26. Above, the total rainfall reaches 127.2 mm. Figure 13 shows that 4 discontinuous low-resistivity areas are located in the source area based on the HDERT method, with three low-resistivity areas located on the ground at the head and one low-resistivity area being in the front of the source area. The resistivity is less than 1203 ohm-m in the low-resistance anomaly areas, where the thicknesses of the aquifer and weak interlayer are 1 to 503 m. The spatial distribution of the weak interlayer at the source area was deduced to be full of water, confirming a "bathtub" type structure. Rainfall infiltration acts to recharge the base of the deposit aquifer. Rainfall-induced landslide occurs at a time when the pore water pressure exceeds the effective normal stress. The resulting excess pore water pressure ensures the shallow subsurface failure and downslope transposition in the source area [33].

4.3.3. The Weak and Impermeable Material in the Subsurface. Through a field investigation and laboratory test data, the upper layer of this slope is composed of crushed stone soil, and the middle layer is the sliding belt, which is mainly a weak loose layer composed of clastic clay. The coefficients of permeability for the crushed rock soil are higher than those for the clastic clay, and the permeability coefficient of the clastic clay is approximately 7.8×10^{-5} cm/s. However, the sliding bed is mainly a weathered granite bedrock, and its permeability coefficient is less than 5.6×10^{-7} cm/s. Thus, the rainfall infiltrates rapidly through the gravel layer to the loose weak layer. However, due to groundwater gathering in the sliding zone and pushing the landslide body, groundwater poured into the rock joints and split them, e.g., the low-resistivity area in front of the source area. As water infiltrated into the back source area, pore water pressure (PWP) in the substrate increases (rise in the water table), and this evidence indicates that water plays an important role in weak and impermeable materials. The PWP may control the shear strength and pore fluid pressure of the slide material (Figure 13).

4.4. The Future Stability Evaluation. The southern slope of the Sucun landslide was a "chair-like" topography in the bedding subsurface, with the upper slope dipping rather steeply towards the valley and a foot substrate material spread over as the more horizontal "landslide-tectonic" (Figures 6, 12, and 13). Moreover, 3 faults developed at the back of the landslide and formed severe cliffs, which are conducive to the catchment (Figures 3 and 8). A bedding zone of clastic soil with rocks was present at the base of the ancient landslide accumulation both on the eastern side and on the western side of the landslide (Figure 8). The landslide deposits filled the Taoyuan creek valley drilling location and geophysical exploration area of the post-disaster landslide control projects. Figure 14 shows that the high-resistivity area in this toe is reduced to a talus that is mainly composed of rubble and blocks. Several low-resistivity areas are also detected by HDERT in the middle layer, which means that the loose deposit with clastic clay may be full of water. Increases in the amount of water result in a gradual decrease in the shear strength of the sliding zone when the sliding zone becomes completely saturated by long, heavy rainfall-induced landslides.

In physical modelling, the initial sliding occurs at 16:48:25, and the burst is located in the middle of the source area. At this time, the injected water amount is 0.313 m^3, that is, the inflow of water when the burst occurs is 1.78 times the total amount of rainfall once in 100 years. However, because water saturated the loose deposits in the source area for a long time, at 17:08:40, a ditch appeared at the surface on the front part of the source area. Then, the ditch continued to expand and formed headward erosion. As a result, a 1.4 m deep and 1.5 m wide landslide was formed in the source area.

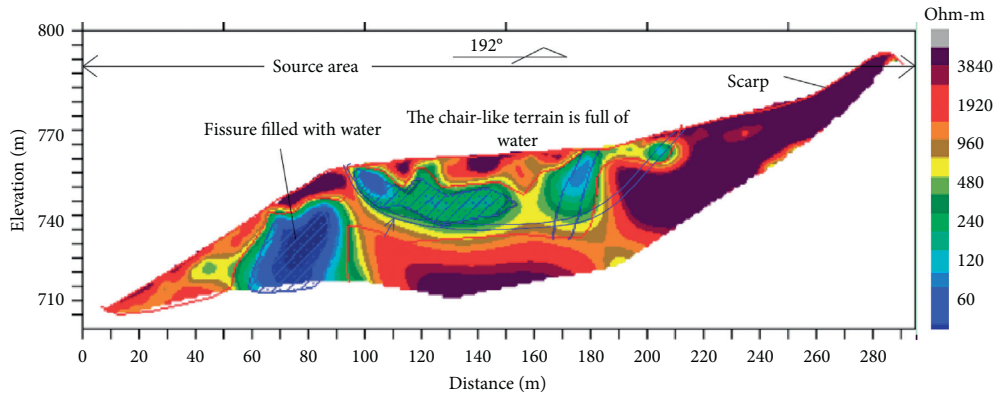

Figure 13: High-density electrical resistivity tomography profiles in the source area (it was taken on September 28, 2016, the topography is like a "chair," and the resistivity shape underground in the back of the source area is like a "bathtub").

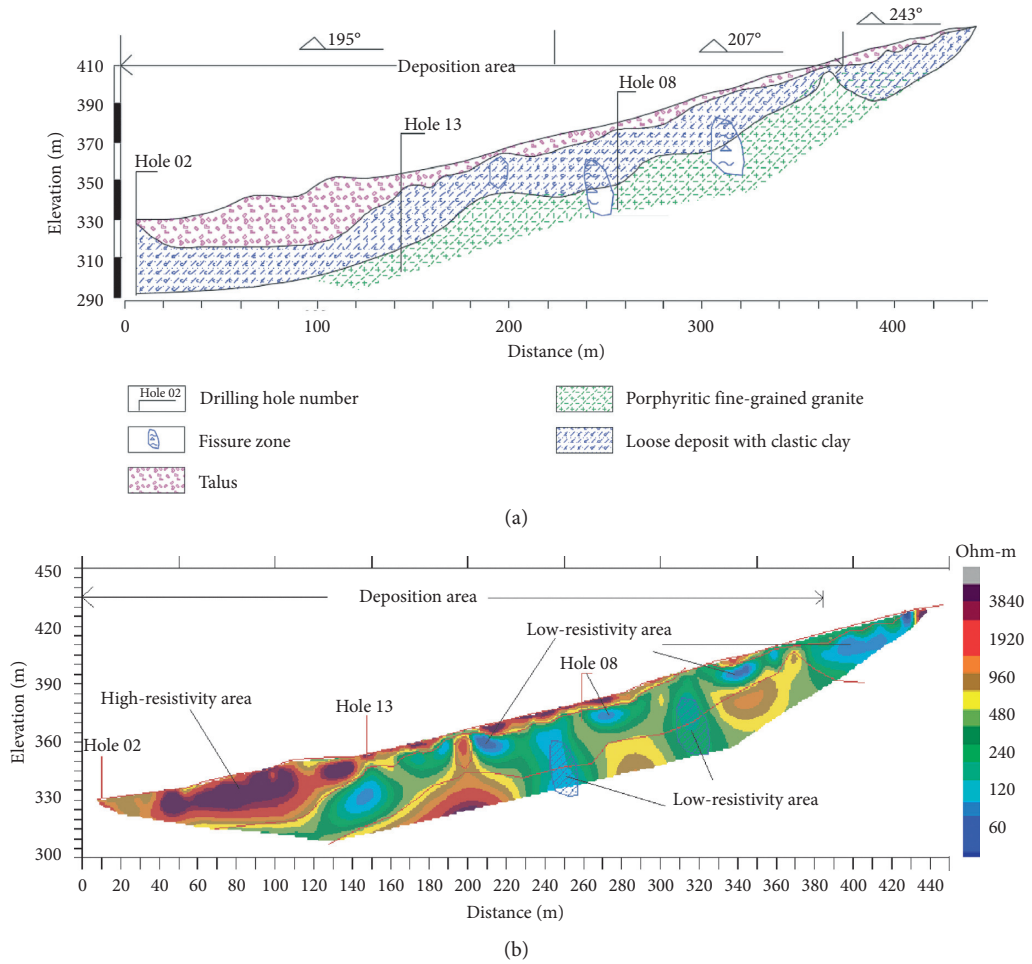

Figure 14: Borehole and HDERT results in the deposition area: (a) borehole profile and (b) HDERT image.

5. Conclusion

Rockslide or avalanches with long-term creep characteristics and unique geological conditions should be considered as the most representative cases, whose landform, geological structure, sediment structure, and composition can fully reflect the dynamic characteristics of the landslide. Depending on multiple methods, this unique information of the Sucun landslide was introduced in this paper, and the cause, formation mechanism, and dynamic characteristics of the Sucun landslide were analyzed. The conclusions are as follows:

(1) The Sucun rock avalanche occurred on the slope behind Sucun after hundreds of years of long-term historical deformation, so this event was not an abrupt event. This rock avalanche was not caused by a single factor rather many complex factors. Long-term rainfall infiltration, the weak interlayer left by the ancient landslide, and the complex landform are the main causes of the landslide. There are sources and unstable slopes that may be involved in the sliding in the research area. When heavy rainfall occurs again, it is highly likely that another landslide will occur.

(2) The "arm-chair" topography of the source area plays an important role in controlling the initial failure of the slope. Because there is a concave topography shaped like a "bathtub" along the trailing edge, the land surface failed first due to the convergence of rainfall infiltration into the ground along the trailing edge. These surface waters are converted into groundwater, forming the excess pore water pressure and supporting the loose rock and soil mass at the rear edge. Then, it is pushed by the continuous collapse at the scarp. The main body accelerates down along the weak interlayer (loose deposit) with an average slope of more than 30° and a length of more than 750 m, gaining a large amount of kinetic energy. These sliding rocks rush upward to the opposite slope, with the landslide speed exceeding 40.11 m/s.

(3) An important lesson we can learn from the catastrophic landslide in Sucun is that people should use caution during rainfall or a typhoon in an ancient landslide area. Special geological conditions, such as landform complexity, formation lithology, and geological structure, are important foundations for landslide formation. From the perspective of disaster prevention and reduction, it is necessary to strengthen the research on the identification and prevention of the landslide under the action of rainfall, especially the corresponding relationship between rainfall and the stability of a slope with weak interlayer bedding. Such catastrophic disasters can be avoided by correctly evaluating the risk of this kind of landslide.

(4) Further studies on the failure mechanism of liquefaction and propagation in the source area, prediction of runout velocity, and runout distance are needed because they are very important parameters for good prevention by the local people. Further analyses are ongoing at the National-Local Joint Engineering Laboratory of Water Engineering Safety and Efficient Utilization of Resources in the Poyang Lake Watershed at the Nanchang Institute of Technology to assess these important factors [34].

Data Availability

Previously reported electronic data in figures were used to support this study and are available in the paper.

Conflicts of Interest

The authors declare that there are no conflicts of interest regarding the publication of this paper.

Acknowledgments

This research was supported by the Open Fund Projects of Jiangxi Engineering Research Center of Water Engineering Safety and Resources Efficient Utilization (no. OF201603), Jiangxi Provincial Key Scientific Research Plan (no. 20177BBG70046), National Key R&D Program of China during the 13th Five-Year Plan Period (no. 2017YFC0804600), the National Natural Science Foundation of China (nos. 41641023 and 51869012), Jiangxi Province Department of Education Science and Technology Research Project (no. GJJ171008), and the Natural Science Foundation of Jiangxi Province (no. 20171BAB213027). The abundant help from the Zhejiang No. 3 Geology Brigade and the Zhejiang Nonferrous Geophysical Technology Application Research Institute is appreciated. The authors thank Chaojun Ouyang for sharing data and discussion.

Supplementary Materials

The supplementary file contains the video of the SU village landslide. (*Supplementary Materials*)

References

[1] S. B. Savage and K. Hutter, "Dynamics of avalanches of granular materials from initiation to runout. Part I: analysis," *Acta Mechanica*, vol. 86, pp. 1–4, 1991.

[2] D. G. Masson, A. B. Watts, and M. J. R. Gee, "Slope failure on the flanks of western Canary Islands," *Earth-Science Reviews*, vol. 57, no. 1-2, pp. 1–35, 2015.

[3] F. C. Dai, C. F. Lee, and Y. Y. Ngai, "Landslide risk assessment and management: an overview," *Engineering Geology*, vol. 64, no. 1, pp. 65–87, 2012.

[4] A. Aryal, B. A. Brooks, and M. E. Reid, "Landslide subsurface slip geometry inferred from 3-D surface displacement fields," *Geophysical Research Letters*, vol. 42, no. 5, pp. 1411–1417, 2015.

[5] D. Huntley, P. Bobrowsky, M. Hendry, R. Macciotta, and M. Best, "Multi-technique geophysical investigation of a very slow-moving landslide near ashcroft, British Columbia, Canada," *Journal of Environmental and Engineering Geophysics*, vol. 24, no. 1, pp. 87–110, 2019.

[6] L. Wang, Y. Yin, B. Huang, Z. Zhang, and Y. Wei, "formation and characteristics of guang'an village landslide in Wuxi, Chongqing, China," *Landslides*, vol. 16, no. 1, pp. 127–138, 2019.

[7] S. Lacasse and F. Nadim, "Landslide risk assessment and mitigation strategy," in *Landslides-Disaster Risk Reduction*, K. Sassa and P. Canuti, Eds., Springer, Berlin, Germany, 2009.

[8] V. C. J. Westen, N. Rengers, and R. Soeters, "Use of geomorphological information in indirect landslide susceptibility assessment," *Natural Hazards*, vol. 30, no. 3, pp. 399–412, 2003.

[9] C.-M. Lo and M.-C. Weng, "Identification of deformation and failure characteristics in cataclinal slopes using physical modeling," *Landslides*, vol. 14, no. 2, pp. 499–515, 2017.

[10] H.-Y. Sun, P. Pan, Q. Lü, Z.-L. Wei, W. Xie, and W. Zhan, "A case study of a rainfall-induced landslide involving weak interlayer and its treatment using the siphon drainage method," *Bulletin of Engineering Geology and the Environment*, vol. 78, no. 6, pp. 4063–4074, 2019.

[11] O. Hungr, S. Leroueil, and L. Picarelli, "The Varnes classification of landslide types, an update," *Landslides*, vol. 11, no. 2, pp. 167–194, 2014.

[12] R. Wei, Q. Zeng, T. Davies et al., "Geohazard cascade and mechanism of large debris flows in Tianmo gully, SETibetan Plateau and implications to hazard monitoring," *Engineering Geology*, vol. 233, pp. 172–182, 2018.

[13] Q. Xu, X. Fan, R. Huang et al., "A catastrophic rockslide-debris flow in Wulong, Chongqing, China in 2009: background, characterization, and causes," *Landslides*, vol. 7, no. 1, pp. 75–87, 2010.

[14] T. Bekler, Y. L. Ekinci, A. Demirci, A. E. Erginal, and C. Ertekin, "Characterization of a landslide using seismic refraction, electrical resistivity and hydrometer methods, adatepe-canakkale, NW Turkey," *Journal of Environmental and Engineering Geophysics*, vol. 16, no. 3, pp. 115–126, 2011.

[15] T. Zhao, G. B. Crosta, S. Utilli, and V. D. Blasio, "Investigation of rock fragmentation during rockfalls and rock avalanches via 3-D discrete element analyses," *Journal of Geophysical Research, Earth Surface*, vol. 122, no. 3, pp. 678–295, 2016.

[16] C.-j. Ouyang, W. Zhao, S.-M. He et al., "Numerical modeling and dynamic analysis of the 2017 Xinmo landslide in Maoxian County, China," *Journal of Mountain Science*, vol. 14, no. 9, pp. 1701–1711, 2017.

[17] C. Ouyang, H. An, S. Zhou et al., "Insights from the failure and dynamic characteristics of two sequential landslides at Baige village along the Jinsha River, China," *Landslides*, vol. 16, no. 7, pp. 1397–1414, 2019.

[18] G. E. Hilley, R. Burgmann, and A. Ferretti, "Dynamics of slow-moving landslides from permanent scatterer analysis," *Science*, vol. 304, no. 5679, pp. 1952–1955, 2004.

[19] P. Hilger, R. L. Hermanns, J. C. Cosse, B. Jocobs, B. Etzelmuller, and M. Krautblatter, "Multiple rock-slope failures from Mannen in Romsdal Valley, western Norway, revealed from Quaternary geological mapping and Be-10 exposure dating," *Holocene*, vol. 28, no. 12, pp. 1841–1854, 2009.

[20] T. Carlà, V. Tofani, L. Lombardi et al., "Combination of GNSS, satellite InSAR, and GBInSAR remote sensing monitoring to improve the understanding of a large landslide in high alpine environment," *Geomorphology*, vol. 335, pp. 62–75, 2019.

[21] N. Casagli, V. Tofani, S. Morelli et al., "UAV and ground-based remote sensing techniques for landslide mapping, monitoring and early warning," *Advancing Culture of Living with Landslides*, vol. 4, no. 9, pp. 1–19, 2017.

[22] X. Chen, T. Ma, C. Li, H. Liu, B. Ding, and W. Peng, "The catastrophic 13 November 2015 rock-debris slide in Lidong, south-western Zhejiang (China): a landslide triggered by a combination of antecedent rainfall and triggering rainfall," *Geomatics, Natural Hazards and Risk*, vol. 9, no. 1, pp. 608–623, 2018.

[23] J. N. Xiong, J. Li, W. M. Cheng, N. Wang, and L. Guo, "A GIS-based support vector machine model for flash flood vulnerability assessment and mapping in China," *ISPRS International Journal of Geo-Information*, vol. 8, pp. 1–23, 2019.

[24] Y. Yu, M. Shen, H. Sun, and Y. Shang, "Robust design of siphon drainage method for stabilizing rainfall-induced landslides," *Engineering Geology*, vol. 249, pp. 186–197, 2019.

[25] B. Li, K. F. Zhou, J. Ye, and P. Sha, "Application of a probabilistic method based on neutrosophic number in rock slope stability assessment," *Applied Sciences-Basel*, vol. 9, no. 11, pp. 1–18, 2019.

[26] D. J. Varnes, "Slope movement types and processes," in *Special Report 176: Landslides: Analysis and Control*, R. L. Schuster and R. J. Krizek, Eds., pp. 11–33, National Academy of Science, Washington, DC, USA, 1978.

[27] M. Borga, G. Dalla Fontana, C. Gregoretti, and L. Marchi, "Assessment of shallow landsliding by using a physically based model of hillslope stability," *Hydrological Processes*, vol. 16, no. 14, pp. 2833–2851, 2002.

[28] R. Sosio, G. B. Crosta, and O. Hungr, "Complete dynamic modeling calibration for the Thurwieser rock avalanche (Italian Central Alps)," *Engineering Geology*, vol. 1100, no. 1-2, pp. 11–26, 2008.

[29] A. Voellmy, "Uber die Zerstörungskraft von Lawinen," *Schweizerische Bauzeitung*, vol. 73, pp. 212–217, 1955.

[30] S. G. Evans and J. J. Clague, "Recent climatic change and catastrophic geomorphic processes in mountain environments," *Geomorphology and Natural Hazards*, vol. 10, no. 1–4, pp. 107–128, 1994.

[31] V. V. Adushkin, S. N. Andreev, and S. I. Popel, "Formation of nano-and microspherules of minerals in ore deposits depending on depth of host rock occurrence," *Geology of Ore Deposits*, vol. 48, no. 3, pp. 237–243, 2006.

[32] A. E. Scheidegger, "On the prediction of the reach and velocity of catastrophic landslides," *Rock Mechanics*, vol. 5, no. 4, pp. 231–236, 1973.

[33] G. E. Stephen, S. M. Gabriele, S. Alexander, and L. H. Reginald, "Landlsides from massive rock slope failure, NATO sciences Series, VI," *Earth and Environmental Sciences*, vol. 49, pp. 115–127, 2006.

[34] S. McDougall, "2014 Canadian Geotechnical Colloquium: landslide runout analysis-current practice and challenges," *Canadian Geotechnical Journal*, vol. 54, no. 5, pp. 605–620, 2017.